

Ice sheet model simulations reveal polythermal ice conditions existed across the NE USA during the Last Glacial Maximum

Joshua Cuzzone<sup>1</sup>, Aaron Barth<sup>2</sup>, Kelsey Barker<sup>2</sup>, Mathieu Morlighem<sup>3</sup>

<sup>1</sup>Joint Institute for Regional Earth System Science and Engineering, University of California, Los Angeles, USA

<sup>2</sup>Department of Geology, Rowan University, Glassboro, USA

<sup>3</sup>Department of Earth Sciences, Dartmouth College, Hanover, USA

Correspondence to: Joshua K. Cuzzone (jcuzzone@ucla.edu)

## Abstract

Geologic [archives](#) of the Laurentide Ice Sheet (LIS) provide abundant constraints on the [size and extent](#) of the ice sheet during the Last Glacial Maximum (LGM) [and throughout the deglaciation](#). Direct observations of LGM LIS thickness are non-existent, however, [due to ice-surface elevations likely exceeding those of even the tallest summits in the Northeastern United States \(NE USA\)](#). [Geomorphic and isotopic data from mountains across the NE USA can inform basal conditions while covered by ice including the presence of warm- or cold-based regimes](#). While warm-based ice and erosive conditions likely existed on the flanks of these summits and throughout neighboring valleys, [cosmogenic nuclide inheritance and frost-riven blockfields on summits suggest ineffective glacial erosion and cold-based ice conditions](#). Geologic [reconstructions indicate that a complex erosional and thermal regime likely existed across the NE USA sometime during and after the LGM](#), although this has not been confirmed by ice sheet models. Instead, current ice sheet models simulate warm-based ice conditions across this region, with disagreement likely arising from the use of low resolution meshes (e.g., >20 km) which are unable to resolve the high bedrock relief across [the NE USA](#) that strongly influenced overall ice flow and the complex LIS thermal state. Here we use a newer generation ice sheet model, the Ice-sheet and Sea-level System Model (ISSM), to simulate the LGM conditions of the LIS across the NE USA and at 3 localities with high bedrock relief (Adirondack Mountains, White Mountains, and Mount Katahdin), with results confirming the existence of a complex thermal regime as interpreted [from the geologic data](#). The model uses [a small ensemble of LGM climate boundary conditions, and a high-resolution horizontal mesh that resolves bedrock features down to 30 meters to reconstruct LGM ice flow, ice thickness, and thermal conditions](#). These results indicate that across the NE USA, polythermal conditions existed during the LGM. While the majority of this domain is simulated to be warm-based, cold-based ice persists where ice velocities are slow (<15 m/yr) particularly across regional ice divides (e.g., Adirondacks). Additionally, sharp thermal boundaries are simulated where cold-based ice across high elevation summits (White Mountains and Mount Katahdin) flank warm-based ice in adjacent valleys. [We find that the elevation of this simulated thermal boundary ranges between 800-1500 meters, largely supporting geologic interpretations that polythermal ice conditions existed across NE USA during the LGM, however this boundary varies geographically](#). In general, we show that a model [using finer spatial resolution compared to older models](#) is able to simulate the polythermal conditions captured in the geologic data, with model output being of potential utility for site selection in future geologic studies and geomorphic interpretation of landscape evolution.

Deleted: evidence

Deleted: s

Deleted: areal

Deleted: with most geologic data across high elevation summits in the

Deleted: often showing signs of cosmogenic nuclide inheritance, indicative of weakly erosive ice flow and the presence of cold-based ice.

Deleted:

Deleted: summit

Deleted: issues have hampered efforts to constrain the timing of the emergence of ice-free conditions at high elevation summits....

Deleted: These

Deleted: Ggeomorphic r

Deleted: southeasternmost extent of the LIS

Commented [MOU1]: Paul suggests broadening – do we say NE USA here?

Deleted: this region

Deleted: by

Deleted: higher-order physics,

Deleted: ,

Deleted: Because geologic data areis geographically limited, these high-resolution simulations can help fill gaps in our understanding of the geographical distribution of the polythermal ice during the LGM.

Deleted: with

Deleted: and higher order physics

## 1. Introduction

During the Last Glacial Maximum (26.5 to 19.0 ka; Clark et al., 2009), global temperatures cooled by ~6.1°C (Tierney et al., 2020) leading to the growth of expansive ice sheets and the lowering of global sea level by ~130 m (Clark & Mix, 2002). As part of the North American Ice Sheet complex (NAIS), the Laurentide Ice Sheet (LIS) is estimated to have contained 75-85 m global sea-level equivalent (SLE; Clark & Mix, 2002) thus representing a climatically and geographically important component of the cryosphere. Extending southwards from its source region in northern Canada, the LIS covered most of the northeastern United States (NE USA; Fig. 1) with its terminal position located along Martha's Vineyard, Massachusetts (MA), Long Island, New York (NY), and into northern New Jersey and Pennsylvania to the west (Dalton et al., 2020). The retreat of the LIS during the last deglaciation is constrained through numerous geochronologic studies including: varve chronologies (Ridge et al., 2012), basal radiocarbon dates (Fig., 1d; Dyke et al., 2004; Dalton et al., 2020), and terrestrial in-situ cosmogenic nuclide surface exposure ages of moraines (Balco and Schaefer, 2006; Bromley et al., 2015; Ullman et al., 2016; Corbett et al., 2017; Hall et al., 2017; Bromley et al., 2020; Drebbler et al., 2023; Halsted et al., 2023; Balter-Kennedy et al., 2024). While these geologic archives constrain ice margin retreat well, the vertical thinning history and ultimately the volumetric change of the LIS during the last deglaciation in this region remains poorly known.

Fortunately, because of the high vertical relief across the NE USA, studies have addressed the vertical thinning history of the LIS in this region by dating glacial features along vertical transects (herein referred to as dipstick studies; Bierman et al., 2015; Koester et al., 2017; Barth et al., 2019; Corbett et al., 2019; Koester et al., 2020; Halsted et al., 2023). Geologic archives such as glacial erratics, striations, and soil development, as well as isotopic evidence from terrestrial cosmogenic nuclide (TCN) surface exposure ages, can be interpreted to reflect subglacial thermal regimes (i.e., cold- or warm-based ice) in the past. Glacial erratics found on the peaks indicate continental ice cover at some point during the Quaternary (De Laski, 1872; Tarr, 1900; Antevs, 1932; Davis, 1989). TCN surface exposure ages from erratics and glacially-affected bedrock on the peaks indicate that rapid vertical ice sheet thinning occurred coincident with ice margin retreat during the last deglaciation, and predominantly during the Bølling-Allerød warm period. Through surface exposure dating of bedrock features and glacial erratics, these dipstick studies commonly find the presence of inherited nuclides across high elevation sites (>1200 m; Halsted et al., 2023), making geologic interpretations of the onset of vertical ice thinning at these locations uncertain. Consequently, these data suggest that the high elevation regions of the NE USA were likely covered by cold-based ice characterized by the absence of subglacial water and ultimately much reduced subglacial erosion, with warm-based ice and erosive conditions flanking the valleys of these high elevation regions (Halsted et al., 2022). Glacial striations and roche moutonnée found below the summits of the Presidential range in New Hampshire (NH) and Mt. Katahdin in Maine (ME) indicate the presence of warm-based ice locally (Goldthwait, 1970; Davis, 1978; 1989; Thompson et al., 2002). Similar evidence with the addition of weakly developed soils on the summits of the Presidential Range indicate cover by erosive, warm-based ice (Goldthwait, 1970).

While these geologic interpretations support the existence of polythermal ice conditions across the NE USA, it is not well known how this subglacial regime varied spatially and whether the existence of this boundary occurred along a geographically consistent elevation. Furthermore, a lack of precise age control for many of these features leaves the question of temporal variability unanswered and whether or not the thermal regime was consistent throughout glaciation and deglaciation. This has implications for interpreting geologic data of past ice sheet retreat or

Deleted: These studies

Deleted: difficult

Deleted: 3

thinning particularly at high elevations, as well as erosional processes that may have operated during glaciation across the NE USA, as erosional patterns are closely related to the ice sheet thermal regime (Lai and Anders et al., 2021). Ultimately, where these geologic archives are limited in their spatial coverage, ice sheet models can be used to simulate broader characteristics of this thermal regime.

Ice sheet models have been important tools to study LIS conditions during the LGM and assess the drivers of deglacial change (Sugden, 1977; Marshall et al., 2000; Hooke and Fastook, 2007; Tarasov and Peltier, 2007; Gregoire et al., 2012; Moreno et al., 2023). Not only can ice sheet models aid in the interpretation of geologic proxies of past ice sheet behavior, but they can provide outputs that enable a more informed choice when considering field locations for sampling. For example, a recent assessment of the basal thermal state of the Greenland Ice Sheet (MacGregor et al., 2016; 2022), which in part relied upon output from newer generation ice sheet models, was used to inform field campaigns aimed at sampling subglacial bedrock in portions of the Greenland Ice Sheet that were estimated to be cold-based with low erosion (Briner et al., 2022).

In regards to the LIS, prior ice sheet modeling efforts were useful in identifying a broad picture of the thermal behavior of the LIS, which indicated that at the LGM roughly 20-50% of the LIS was warm based (Marshall and Clark, 2002; Tarasov and Peltier, 2007), including the NE USA. Some aspects of these simulations (Tarasov and Peltier, 2007) do agree well with broad scale geomorphic indicators of basal conditions (Klemen and Hattestrand, 1999; Briner et al., 2006; Klemen and Glasser, 2007; Briner et al., 2014), which indicate that the LIS exhibited a varying subglacial thermal regime, with frozen bed patches interspersed particularly along ice divides and in some cases residing along sharp boundaries with warm-based ice streams or outlet glaciers.

However, due to the low spatial resolution of existing models (>20 km), the high topographic relief across the NE USA is poorly resolved and therefore the sharp thermal boundary between cold and warm-based ice identified in the geologic archives is not captured. This is likely due to the more coarsely resolved models' inability to capture advective and diffusive processes at these small spatial scales. Likewise, as the high relief of this region served as a control and impediment to ice flow during the LGM, the impacts of ice flow on deformational and frictional heating is more poorly captured in lower resolution models. This can be improved by downscaling ice sheet models to higher resolution, which has shown promise (Staiger et al., 2005) in interpreting how polythermal ice conditions may have influenced regional glacial geomorphology.

To address this shortcoming, we use a high-resolution ice sheet model to simulate the thermal regime of the LIS across the NE USA during the LGM. Our model experiments are designed to test whether the presence of this sharp thermal regime is simulated and to assess the spatial and elevational characteristics of the basal thermal regime at regional and local scales (i.e., mountain range) where geologic archives suggest the existence of polythermal conditions. Through this work, we aim to evaluate current geologic interpretations, while also filling gaps in our understanding of this complex thermal regime where geologic constraints are limited.

## 2. Methods

The NE USA (Figure 1), is marked by high topographic relief that spans an elevational range from sea-level to >1500 meters. In order to capture these large gradients in bedrock topography and thermal boundaries within the ice sheet, we employ a nested modelling approach (Briner et al., 2020; Cuzzone et al., 2022), whereby a more coarsely resolved and larger model

Deleted: evidence

Deleted: suggests

Deleted: support

Deleted: A, comprising of the states listed in

Deleted:

172 provides boundary conditions necessary for downscaling over regional and local scale domains  
 173 that are more finely resolved (see Figure S1).  
 174

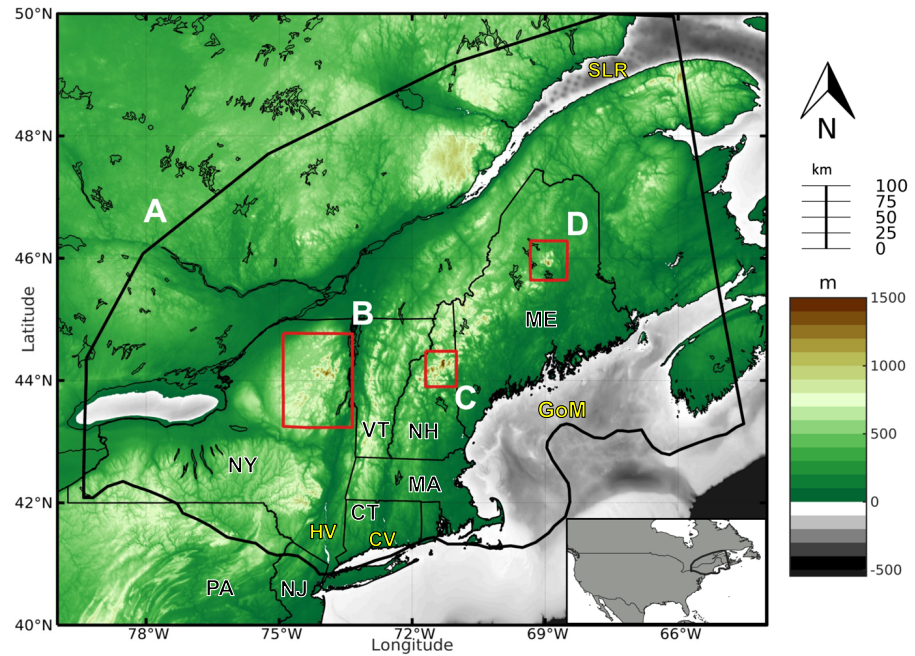


Figure 1. Bedrock topography (meters) and model domains for the regional NE USA ice sheet model (shown as black outline; A) and the local scale models shown in the red outlines across the Adirondack Mountains (B), White Mountains (C) and Mount Katahdin (D). The southern boundary of the NE USA model (A) follows the reconstructed LGM ice extent at the LGM from Dalton et al. (2020). States are abbreviated as: PA: Pennsylvania, NJ: New Jersey, CT: Connecticut, NY: New York, MA: Massachusetts, VT: Vermont, NH: New Hampshire, ME: Maine HV: Other locations described in the text are abbreviated as: Hudson Valley, CV: Connecticut Valley, GoM: Gulf of Maine, SLR: Saint Lawrence River Valley.

### 2.1.1 Ice Sheet Model

We use the Ice-sheet and Sea-level System Model (ISSM; Larour et al., 2012), a higher-order thermomechanical finite-element ice sheet model to simulate the LIS LGM conditions across the NE USA. Because of the high topographic relief across this region and associated impact on ice flow, we use a higher-order approximation to solve the momentum balance equations (Dias dos Santos et al., 2022). This ice flow approximation is a depth-integrated formulation of the higher-order approximation of Blatter (1995) and Pattyn (2003), which allows for an improved representation of ice flow compared with more traditional approaches in paleo-ice flow modelling (e.g., shallow ice approximation or hybrid approaches).

An enthalpy formulation that simulates both temperate and cold-based ice (Aschwenden et al., 2012; Serrousi et al., 2013; Rückamp et al., 2020) is used to capture the thermal state of the ice sheet. Our model contains four vertical layers and uses quadratic finite elements ( $P1 \times P2$ ) along the  $z$  axis for the vertical interpolation following Cuzzone et al. (2018) in order to better capture sharp thermal gradients near the base and simulate the vertical distribution of temperature within the ice. This methodology has been successfully applied to simulate the transient behavior of the Greenland Ice Sheet across geologic timescales and the contemporary period (Briner et al., 2020; Smith-Johnsen et al., 2020; Cuzzone et al., 2022). The ice rheology follows Glen's flow law with the ice viscosity being dependent on the simulated ice temperature following rate factors in Cuffey and Paterson (2010). Surface temperature (see 2.1.3) and geothermal heat flux (Shapiro and Ritzwoller, 2004) are imposed as boundary conditions in the thermal model. We use a linear friction law (Budd et al., 1979), where the basal drag ( $\tau_b$ ) is represented as:

$$\tau_b = -\alpha^2 N u_b \quad (1)$$

where  $\alpha$  represents the spatially varying friction coefficient,  $N$  represents the effective pressure, and  $u_b$  is the basal velocity. Here  $N = g(\rho_i H + \rho_w Z_b)$ , where  $g$  is gravity,  $H$  is ice thickness,  $\rho_i$  is the density of ice,  $\rho_w$  is the density of water, and  $z_b$  is bedrock elevation following Cuffey and Paterson (2010).  $N$  evolves as the ice sheet thickness changes. The spatially varying friction coefficient ( $\alpha$ ) is constructed as a function of bedrock elevation above sea level (Åkesson et al. 2018; Cuzzone et al., 2024):

$$\alpha = 200 \times \frac{\min[\max(0, z_b + 600), z_b]}{\max(z_b)} \quad (2)$$

where  $z_b$  is the height of the bedrock with respect to sea level. Using this parameterization, basal friction is larger across high topographic relief and lower across valleys and areas below sea level, which is consistent with what is found today for the Greenland Ice Sheet. The thermomechanical coupling captures the impact of ice deformation and frictional heating on ice temperature, which in turns affect the ice rheology through the temperature dependent rate-factor. In our approach, the friction coefficient is independent of the thermal state but [this](#) has been explored recently in modeling LIS LGM conditions (Moreno et al., 2023). Although it is found to have a measurable impact the overall simulated LGM ice volume, basal temperatures, and ice stream extent particularly for Hudson Bay, these variations are small when compared with uncoupled simulations particularly across the NE USA.

The motion of the ice front is tracked using the level-set method described in Bondzio et al. (2016) and calving is simulated where the LIS interacts with the ocean based on the Von Mises stress criterion (Morlighem et al., 2016). This approach approximates the calving rate as a function of the tensile stresses simulated with the ice, with ice front retreat occurring when the von Mises tensile strength exceeds user defined stress thresholds set for tidewater (1 MPa) and floating ice (200 kPa). These values are consistent with other contemporary and paleo ice sheet modeling studies (Bondzio et al., 2016; Morlighem et al., 2016; Choi et al., 2021; Cuzzone et al., 2024).

Glacial isostatic adjustment (GIA) is not simulated transiently, but is instead prescribed by using a reconstruction of relative sea level from a global GIA model of the last glacial cycle (Caron et al., 2018). Bedrock vertical motion, eustatic sea-level, and geoid change at the LGM are applied to our model to account for GIA (Briner et al., 2020; Cuzzone et al., 2024).



### 2.1.2 Model Domains

To constrain the model boundary conditions necessary for simulating the LIS conditions across the NE USA at both a regional (Figure 1; Domain A) and local scales across the Adirondack mountains, White Mountains, and Mount Katahdin (Figure 1; Domain B-D), we first simulate the LGM ice conditions across the LIS (Figure S1). Our model domain follows the LGM ice extent reconstructed from Dalton et al. (2020) but does not include the Cordilleran Ice Sheet and the connection between Ellesmere Island and the Greenland Ice Sheet. The LIS model is built on a structured mesh with a spatial resolution of 20 km. Bedrock topography is initialized from the General Bathymetric Chart of the Oceans (GEBCO; GEBCO Bathymetric Compilation Group, 2021), which relies on the 15 arcsecond (450-meter resolution) Surface Radar Topography Mission data (SRTM15\_plus; Tozer et al., 2019) for the terrain model. The regional ice sheet model domain (Figure 1, Domain A; Figure S1, Domain 2) covers the NE USA and extends into portions of southern and maritime Quebec. Across this domain anisotropic mesh adaption is used to construct a non-uniform mesh that varies based upon gradients in bedrock topography from GEBCO. The spatial resolution varies from 5 km in areas of low topographic relief, where gradients in bedrock topography are low, to 500 meters in areas of high topographic relief. To gain a more detailed reconstruction of the LGM conditions across the NE USA that are more consistent with the spatial scales associated with the geologic archives (Halsted et al., 2023), we dynamically downscale our results to three local areas within the NE USA (Section 2.2; step 3): the Adirondack Mountains, New York; the White Mountains, New Hampshire; and Mount Katahdin, Maine. The local scale models (Figure 1, Domains B-D; Figure S1, Domain 3) also rely on anisotropic mesh adaptation with spatial resolution varying from 400 to 30 meters based upon topography from the 1 arcsecond (~30-meter resolution) SRTM product (Farr et al., 2007). The three locations were chosen based on their geomorphic qualities, as each represents three of the highest peaks in the NE USA, and has pre-existing geochemical data on glaciation (e.g., cosmogenic surface exposure ages; Bierman et al., 2015; Barth et al., 2019). At these spatial scales, the model is able to resolve the high topographic relief found between the mountain peaks and neighboring valley floors.

Deleted: geomorphic data

Deleted: the highest peak within their respective state

Deleted: geologic

### 2.1.3 Climate Forcing and Surface Mass Balance scheme

Output of monthly mean LGM temperature and precipitation from 5 different climate models is used as surface boundary conditions and to estimate the surface mass balance (SMB). The LGM climate from the TraCE-21ka transient simulation of the last deglaciation is used (Liu et al., 2009; He et al., 2013), as well as output from 4 models participating in the Paleoclimate Modelling Intercomparison Project 4 (PMIP4; Kageyama et al., 2021). The simulated climate from these models differs both with respect to the magnitude and spatial distribution of glacial temperature and precipitation change relative to the preindustrial climate (Figure S2). By using a diversity of surface climate forcings rather than the multi-model mean, we aim to construct a small ensemble of results for the simulated LGM conditions across our model domains as the representative climate model spread can impact the simulated ice sheet geometry, ice flow, and thermal characteristics (Lai and Anders, 2021).

Model	Spatial Resolution	Reference
CCSM4 (TraCE-21ka)	3.75° x 3.75°	Liu et al., 2009 He et al., 2013
MPI-ESM1.2 (MPI)	1.8° x 1.8°	Mauritsen et al., 2019
MIROC-ES2L (MIROC)	2.8° x 2.8°	Ohgaito et al., 2021

		Hajima et al., 2020
IPSLCM5A2 (IPSL)	3.8° x 1.9°	Sepulchre et al. (2020)
AWIESM2 (AWI)	1.8° x 1.8°	Sidorenko et al. (2019)

Table 1. List of climate models used for the LGM surface climate forcing and the corresponding spatial resolution.

We use a positive degree day model (Tarasov and Peltier, 1999; Le Morzadec et al., 2015; Cuzzone et al., 2019; Briner et al., 2020) to calculate the SMB. Our degree day factor for snow melt is  $5 \text{ mm } ^\circ\text{C}^{-1}\text{day}^{-1}$  and  $9 \text{ mm } ^\circ\text{C}^{-1}\text{day}^{-1}$  for bare ice melt, and we use a lapse rate of  $5^\circ\text{C}/\text{km}$  to adjust the temperature of the climate forcings to surface elevation (Abe-Ouchi et al., 2007). The hourly temperatures are assumed to have a normal distribution, of standard deviation  $3.5^\circ\text{C}$  around the monthly mean. An elevation-dependent desertification is included (Budd and Smith, 1981), which reduces precipitation by a factor of 2 for every kilometer change in ice sheet surface elevation and the model accounts for the formation of superimposed ice following Janssens and Huybrechts (2000). The degree day model requires inputs of monthly temperature and precipitation. We apply a commonly used modeling approach to scale a contemporary climatology of temperature and precipitation back to the LGM ('Anomaly Method'; Pollard et al., 2012; Seguinot et al., 2016; Golledge et al., 2017; Tigchelaar et al., 2019; Briner et al., 2020; Cuzzone et al., 2022). The monthly mean climatology of temperature and precipitation for the period 1979-2010 from the European Center for Medium-Range Weather Forecasts ERA5 reanalysis (Hersbach et al., 2020) is bilinearly interpolated onto our model mesh. Next, anomalies of the monthly mean temperature and precipitation fields from the climate models (Table 1), computed as the difference between the LGM and preindustrial control run, are added to the contemporary monthly mean climatology to produce the monthly temperature and precipitation fields at LGM.

## 2.2 Experimental Setup

Our downscaling approach is conducted over 3 steps:

*Step 1 (LIS models; Figure S1 and S3):* First, we construct a model of the LGM LIS using a 2d model with setup described above, and prescribe constant LGM climate (section 2.1.3). Following Moreno et al. (2023), we initialize our model with ice thicknesses of 1000 m north of  $50^\circ\text{N}$ , and allow the simulated LIS to reach equilibrium with respect to ice volume ( $\sim 50,000$  years). The resulting models (ice geometry and velocity) are used to initialize a 3d model that extrudes the 2d model to 4 vertical layers ( $P1 \times P2$  vertical finite elements; section 2.1.1). The thermal regime is assumed to be in steady-state with the LGM climate, and we perform a thermomechanical steady state calculation with a fixed ice sheet geometry and impose surface temperature as Dirichlet boundary conditions until the ice sheet velocities are consistent with ice temperature (i.e., convergence) following Seroussi et al. (2013). Lastly, we let the 3d LIS model relax an additional 20,000 years (i.e., until thermal equilibrium is reached) with the LGM climate as the model adjusts to the updated ice temperature and rheology.

*Step 2 (NE USA models; Figure 1):* We construct our 3d NE USA ice models following the setup discussed in section 2.1 and initialize the model with ice geometry, temperature and rheology, and velocity from the resulting LGM 3d LIS model. Boundary conditions of temperature, ice velocity, and thickness from the LIS results are imposed as Dirichlet boundary conditions at the western, northern, and eastern boundaries following Cuzzone et al. (2022). The initial ice velocity and temperature are downscaled across this domain by performing a thermomechanical steady state

calculation (Seroussi et al., 2013). The model is then allowed to relax with constant LGM climate for 20,000 years as the ice geometry, flow, and temperature adjust to the higher resolution grid.

*Step 3 (local models; Figure 1):* Similar to *Step 2*, the local scale models are initialized with ice geometry, temperature and rheology, and flow with the results from the NE USA model, and boundary conditions (as in *Step 2*) are applied from the NE USA model to the local scale models at the North, South, East, and West boundaries. After running a thermomechanical steady state calculation, the model is allowed to relax to steady-state with constant LGM climate as the ice geometry, flow, and temperature adjust to the higher resolution grid.

Deleted: for 20,000

Deleted: years

Our approach above makes use of the thermomechanical steady state calculation to avoid high computational expense in relaxing the 3d models for a sufficiently long time (e.g. >100,000 yr) until thermal equilibrium is reached. This methodology has been applied to study the basal temperature of present-day ice sheets (Seroussi et al., 2013; MacGregor et al., 2016; 2020), and although it assumes the ice sheet is in equilibrium with climate, we acknowledge that the thermal conditions of the LIS during the LGM likely reflect transiently evolving ice geometry and climatic conditions experienced during the growth and advance to the LGM maximum. For this study, we focus the discussion of our results on the simulated LGM state of the NE USA (step 2) models and local models (step 3), but provide Figure S3 to illustrate the simulated LGM state for the LIS (step 1).

### 3. Results

#### 3.1 Northeast USA

We simulate a range of possible LGM states given different climatologies, and do not specifically tune our models to match reconstructions of ice extent or flowlines. The southern boundary of our model domain is constrained to the maximum reconstructed LGM ice extent from Dalton et al. (2020). In total we have 5 different simulations of the LIS across the NE USA during the LGM (Figure S4), driven by the independent climate forcings (Table 1). The depth integrated ice velocity and ice thickness for the ensemble mean (n=5) of those experiments is shown in Figure 2. Individually, most of the experiments simulate an LGM ice margin that reaches the reconstructed terminal LGM ice extent (Figure 2B & S4) from Dalton et al. (2020), although some simulate reduced ice extent particularly along the southern and eastern boundaries (Figure S4). Thinner ice (<500 m) is found along the ice margin and marine terminating portions of the Atlantic Ocean and Gulf of Maine, and thickens to upwards of 3500 m over the Northwest portion of the model domain. Across the Northwest region, ice velocities are slow (<20 m/yr), consistent with a northward trending ice divide simulated through Quebec (see Figure S3). Additionally, a regional ice divide is simulated across the Adirondack mountains (Figure 2A), where ice velocities are <15m/yr and ice flow vectors indicate diverging ice flow to the southwest and southeast. This regional ice divide is simulated for all experiments (Figure S4), with variation in the magnitude of the ice velocities (~1-25 m/yr). Faster ice flow (>50 m/yr) is found along the ice margin and through areas of topographic troughs. Horizontal ice flow is fastest in marine terminating portions such as the Gulf of Maine (GoM; Figure 1), the St. Lawrence River (SLR; Figure 1), and throughout lower terrain such as the Hudson and Connecticut river valley (Figure 2A; HC, CV Figure 1), with speeds approaching and exceeding 300 m/yr.



367

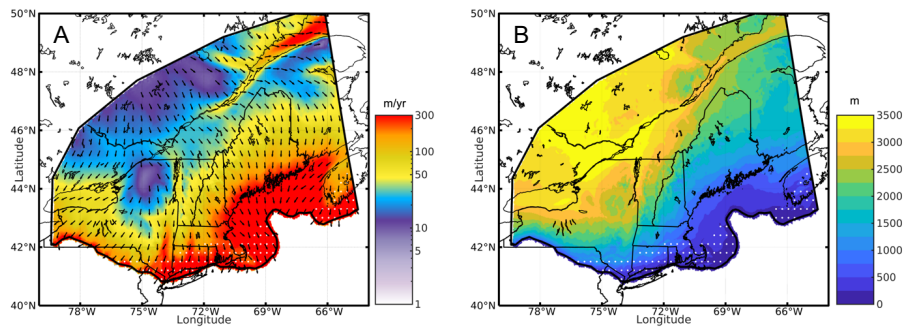


Figure 2. The modeled mean ( $n = 5$ ; Table 1), simulated LGM depth-integrated ice velocity (A; m/yr) and simulated LGM ice thickness (B; m) across the NE USA. Vectors (A) illustrate the simulated direction of ice flow, and colors denote the magnitude of ice velocity. White stippling indicates where areas where some individual models (see Figure S4) simulate no LGM ice cover.

368

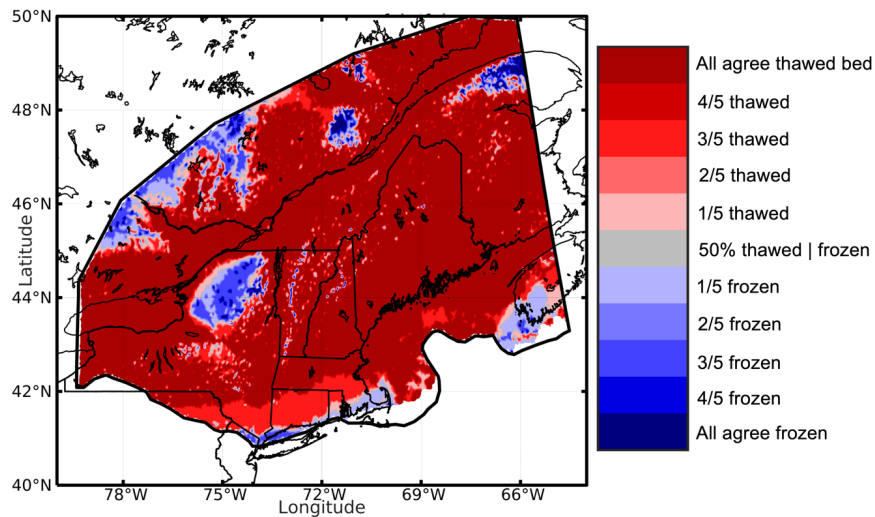


Figure 3. The agreement in the simulated LGM basal thermal state ( $n = 5$ ) for the experiments with varying climate forcing. We assume a thawed bed is present when the pressure corrected  $T_{\text{bed}} \geq -1^\circ\text{C}$  and frozen bed is present when  $T_{\text{bed}} < -1^\circ\text{C}$  following MacGregor et al., 2022.

369

370

For each experiment, we calculate the simulated basal temperature, adjusted for pressure melting (i.e., pressure corrected temperature). Following MacGregor et al. (2022), we consider a

thawed bed to be simulated where the pressure corrected  $T_{bed} \geq -1^{\circ}\text{C}$  and frozen where  $T_{bed} < -1^{\circ}\text{C}$ . The magnitude of the simulated thawed and frozen bed conditions varies across our model domain (Figure S4) but follow a spatial pattern that can be summarized in Figure 3, where we show the inter-model agreement between experiments for thawed and frozen bed conditions. We find that approximately 70% of the model domain is thawed and only 2% of the model domain has frozen bed conditions (i.e., area of domain where all experiments agree), indicating that warm-based ice conditions prevailed across this portion of the LIS.

Warm-based areas are coincident with areas of fast ice flow (Figure 2A), where sliding dominates. Frozen bed conditions are generally simulated in areas of reduced ice flow ( $<15$  m/yr; Figure 2A), particularly along the ice divide that exists in the northwest portion of the model domain, south of the St. Lawrence River, and across the Adirondack mountains. Additionally, the regional model simulates the presence of cold-based ice scattered across areas of high bedrock elevation (see Figure 1 for topographic map). In general, each experiment using the different climate surface forcings simulate a similar spatial pattern of warm-based and cold-based ice (Figure S4). Where each experiment disagrees is with respect to the magnitude of basal cooling, with some experiments simulating both colder basal temperatures and a wider swath of frozen bed conditions primarily across the Adirondack Mountains (Figure S4; TraCE-21ka, MPI, and IPSL). This is likely related to the differences in the simulated LGM surface climate between each climate model. The experiments which simulate a larger swath of frozen bed conditions across the Adirondack Mountains (Figure S4; TraCE-21ka, MPI, and IPSL) have a higher magnitude of simulated LGM surface cooling and higher SMB (Figure S5; TraCE-21ka, MPI, and IPSL), versus the experiments which simulate less extensive frozen bed conditions across the Adirondack Mountains (Figure S4 and S5; MIROC and AWI).

### 3.2 Local Models

#### 3.2.1 Adirondacks

The simulated mean ( $n=5$ ) LGM conditions for the Adirondacks are presented in Figure 4. High topographic relief that exceeds 1000 m is characteristic of the Adirondack Mountains, with 43 mountain peaks exceeding 1200 m in elevation, and maximum elevations reaching 1600 m (Figure 4; HPA: High Peaks area). Simulated LGM ice thickness reaches between 1600 m to 2000 m across the highest peaks, increases throughout the lower valleys in excess of 2000 m, and reaches upwards of 3000 m across the lower elevations in the Northwest and Northeast portion of the domain (Figure 4C). Consistent with the ice divide simulated in the regional model (Figure 2), slow ice velocities ( $<10$  m/yr to 25 m/yr) dominate across the Adirondacks (Figure 4D). Ice flow generally trends in a south-southeastward direction, with ice velocities increasing to  $> 60$  m/yr across lower elevation valleys. Approximately 58% of the model domain is thawed and 4% of the model domain has frozen bed conditions (i.e., area of domain where all experiments agree), indicating that warm-based ice conditions prevailed across this portion of the LIS (Figure 4E). Generally, frozen bed conditions are confined to high elevation peaks (Figure 4B), where low ice velocities and thinner ice exist, making these high elevation regions more susceptible to vertical advection of cold surface temperature (LGM temperature range from climate models:  $-24^{\circ}\text{C}$  to  $-18^{\circ}\text{C}$ ). However, we also find that across lower elevation regions, particularly in the Northwest portion of the domain, frozen bed conditions are simulated. Here ice is thick (upwards of 3000 m; Figure 4A) but is characterized by very slow ice flow ( $<10$  m/yr). Without limited frictional and deformational heating, this area was likely influenced by the vertical advection of cold surface climate despite thick ice. Across this domain the thermal boundary separating frozen and thawed

bed (Figure 4E) is 880 m. However, if we just consider the High Peaks area (HPA; Figure 4A), that thermal boundary resides at 1180 m.

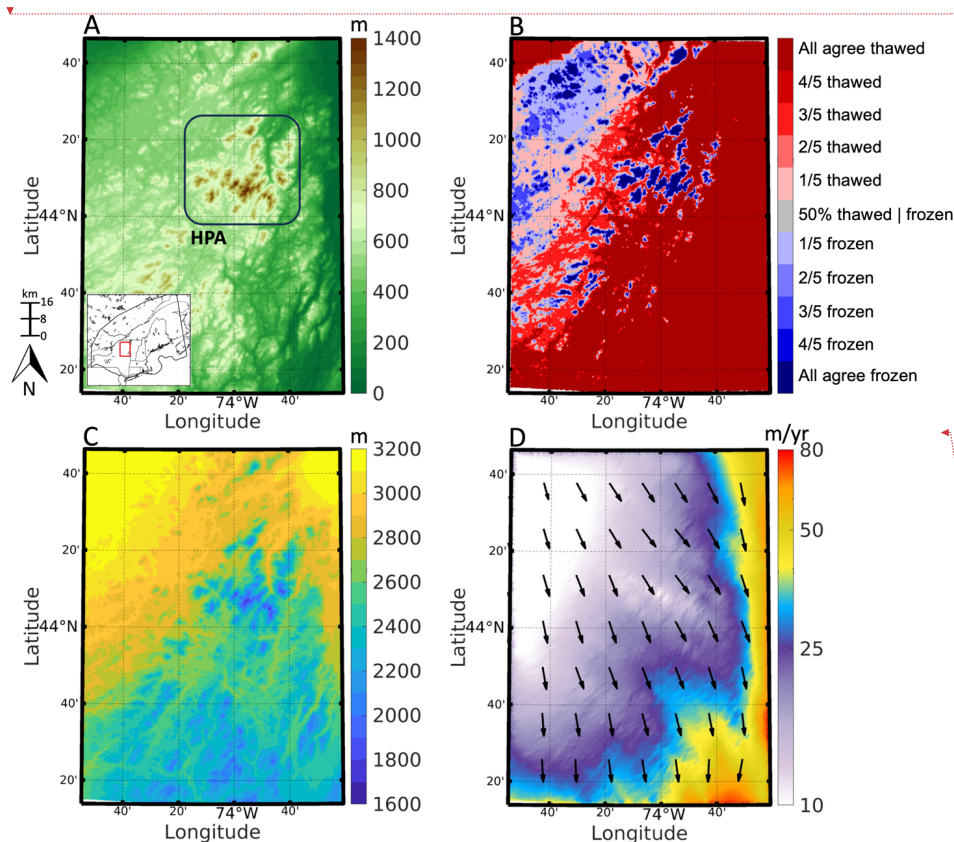


**Figure 4.** A) Bedrock topography for the Adirondack Mountains (m). Box highlights the High Peaks area. See inset in Figure 4A for geographical context within the NE USA. E) Modeled agreement for simulated frozen and thawed bed conditions. C) The model mean ice thickness (m). D) The model mean depth average ice velocity (m/yr). Note, vectors denote ice flow direction and not the magnitude of velocity.

### 3.2.2 White Mountains

To the east of the Adirondack Mountains, the White Mountains comprise a series of mountain ranges intersected by deeply incised valleys, with the highest peak Mount Washington reaching 1912 m (Figure 5A). The simulated mean LGM conditions for the White Mountains are presented in Figure 5. Ice thickness ranges between 600 m to 1200 m across high elevations peaks (Figure 5C) and thickens to 2000 m in the deeply incised valleys. Across the lower elevations in the Northwest portion of the model domain (Figure 5A), ice thickness reaches upwards of 2500

Deleted: 2

Deleted:

Formatted: Keep with next

Deleted: ¶

m. Ice flows southeastward across this region, with simulated ice velocities being higher than is found across the Adirondack Mountains. Ice velocities are lowest in the Northwest portion of the domain and across Mount Washington, where the southeastward ice flow is impeded by the high

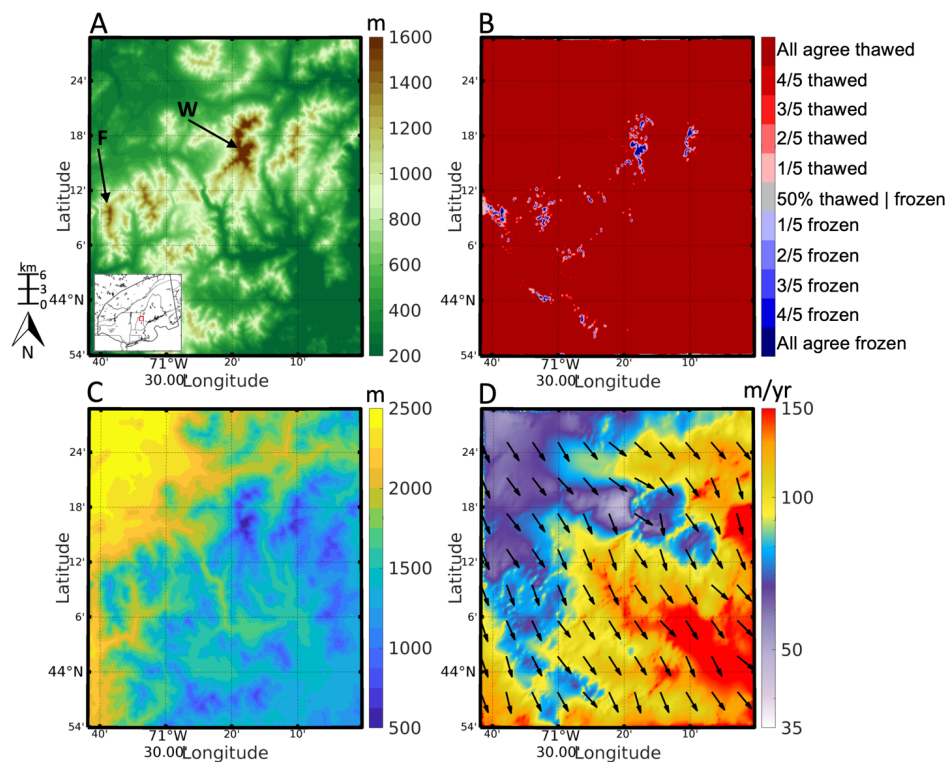


Figure 5. A) Bedrock topography for the White Mountains (m). Highlighted are Mt. Washington (W) and Mount Lafayette and Little Haystack Mountain, labeled (F) for Franconia Range. See inset in Figure 5A for geographical context within the NE USA. B) Modeled agreement for simulated frozen and thawed bed conditions. C) The model mean ice thickness (m). D) The model mean depth average ice velocity (m/yr). Note, vectors denote ice flow direction and not the magnitude of velocity.

elevation bedrock (35 – 60 m/yr; Figure 5D), and increases up to 150 m/yr across the lower elevations in the southeast region. When considering the basal thermal regime, we find that 95% of the model domain has thawed bed conditions, with only 0.5% of the domain having frozen bed conditions. Frozen bed conditions are limited to high elevation sites, particularly across the Presidential Range where Mt. Washington is located and Mount Lafayette and Little Haystack in the Franconia Range, with a mean thermal boundary between frozen and thawed bed conditions residing at 1530 m.

446  
447  
448  
449  
450  
451  
452  
453  
454  
455  
456  
457  
458  
459  
460

### 3.2.3 Mount Katahdin

Mount Katahdin reaches 1606 m with upwards of 1300 m of relief above the surrounding valleys (Figure 6A). The simulated mean LGM conditions for Mount Katahdin are presented in Figure 6. Across the summit of Mount Katahdin, ice thicknesses reach between 500-700 m, and thicken to 1500 - 2000 m around the flanks of the mountain (Figure 6C) and the surrounding lowlands. The ice generally flows south-southeastward (Figure 6D), with ice flow diverging and slowing down to 25 m/yr upstream of Mountain Katahdin, before reaching a minimum of 10-15 m/yr at the summit. Ice flow converges on the downstream side of Mount Katahdin and reaches 50-100 m/yr across the lower elevations to the south and east. The simulated basal thermal regime indicates that approximately 97% of the domain is thawed (Figure 6E), with only a few locations across the summit of Mount Katahdin having frozen bed conditions, representing ~0.5 % of the model domain. The elevational boundary separating frozen and thawed bed conditions across this domain is simulated to be at 1320 m.

Deleted:

Deleted: 18

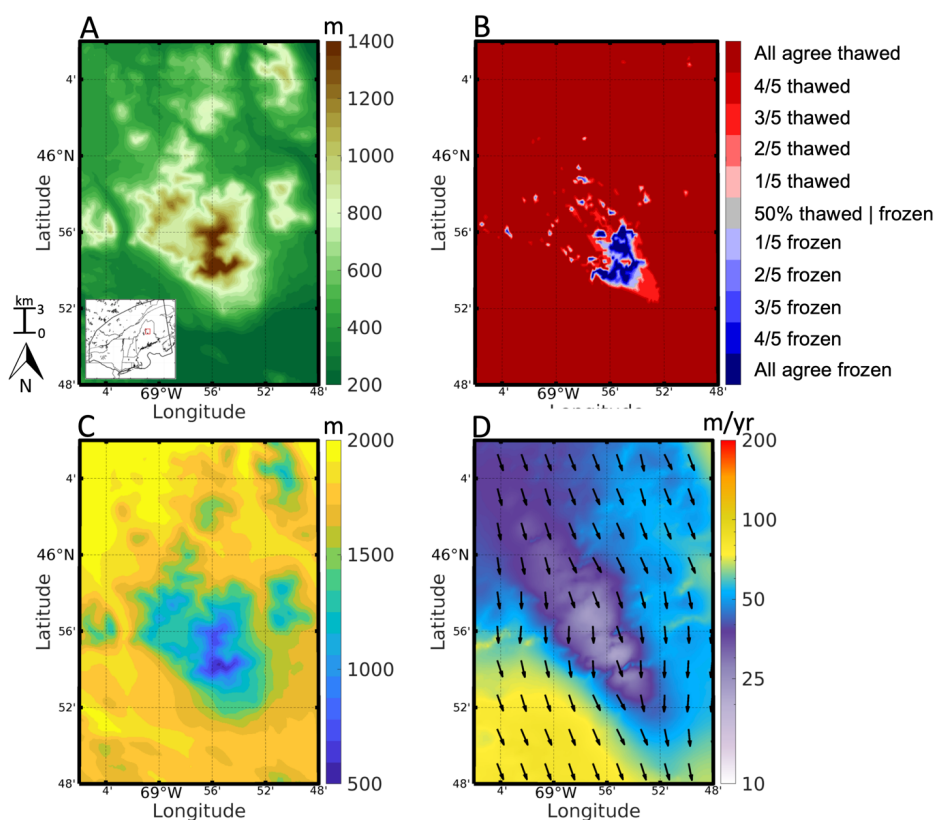


Figure 6. A) Bedrock topography for the Mount Katahdin (m). See inset Figure 6A for geographical context within the NE USA. B) Bedrock topography for Mount Katahdin with an overlay of areas where the models agree (n=5) on simulated frozen and thawed bed conditions. C) The model mean ice thickness (m). D) The model mean depth average ice velocity (m/yr). Note, vectors denote ice flow direction and not the magnitude of velocity.

**Deleted:** A) Bedrock topography for Mount Katahdin (m). See Figure 1 for geographical context within the NE USA. B) Bedrock topography for Mount Katahdin with an overlay of areas where the models agree (n=5) on simulated frozen and thawed bed conditions. C) The model mean ice thickness (m). D) The model mean depth average ice velocity (m/yr). Note, vectors denote ice flow direction and not the magnitude of velocity. E) Modeled agreement for simulated frozen and thawed bed conditions.

**Deleted:**   
<object>

#### 4. Discussion

Across the broader LIS, geomorphic and cosmogenic isotopic evidence supports the existence of frozen bed conditions interspersed amongst regions of warm-based ice (Klemen and Hattestrand, 1999; Klemen and Glasser, 1997; Marquette et al., 2004) and along southern sectors of the LIS, where ice cover was thin (Colgan et al., 2002). More regional indicators of polythermal conditions with sharp contacts of warm-based ice in fast flowing outlet glaciers and cold-based ice on slow moving ice on uplands have been found across Arctic Canada and Baffin Island (Davis et



al., 1999; Marsella et al., 2000; Davis et al., 2006; Briner et al., 2006; 2014; Corbett et al., 2016). Prior to direct evidence from surface exposure dating (Bierman et al., 2015), it was unknown if cold-based ice may have existed across the NE USA. Ice sheet models have been used to infer the basal thermal conditions of the LIS, with implications for better understanding large-scale and regional ice flow and controls on ice mass evolution and regional geomorphology (Sugden et al., 1977; Marshall and Clark, 2002; Tarasov and Peltier, 2007; Moreno-Parada et al., 2023). However, while these models provide possible scenarios for LGM and the deglacial evolution of the LIS thermal state, the coarse spatial resolution of existing models limits the ability to capture sharp thermal gradients that may have existed in high relief terrain, with models simulating large scale warm-based conditions during the LGM across the NE USA (Tarasov and Peltier, 2007). Our downscaled, local simulations agree with geologic interpretations (Davis, 1989; Bierman et al., 2015; Corbett et al., 2018; Halsted et al., 2023) that suggest cold-based ice existed across areas of high relief in the NE USA and the existence of polythermal ice for the region during the LGM. While the majority of this region was exposed to warm-based ice conditions (70%; Figure 3), frozen bed conditions are simulated across areas of low ice velocity (i.e. ice divides) and high elevations (2% of area in Figure 3). It is worth noting that while the focus of this study was on the NE USA, areas of frozen bed ice conditions are simulated for portions Maritime Canada (Figure 3), which agree reasonably well with geologic interpretations from this region (Olejczyk and Gray, 2007).

Because a majority of the geologic data constraining the thermal regime of the LIS across this region are found in areas of high relief, we focused our modeling on three specific locations. Regionally, geologic interpretations posit that the Adirondack Mountains may have acted as an impediment to the south-southeast flow of the LIS during glacial expansion and the LGM (Franzi et al., 2016). Our simulations suggest that ice flow across this region was slow (<15 m/yr; Figure 2A, 4A) in response to a divergence of ice flow around the mountainous terrain. Consequently, a regional ice divide and frozen bed conditions are simulated across portions of this region where ice velocities are <10 m/yr and in areas where the bedrock relief is high. This is further supported by the individual model experiments. Those experiments with colder LGM boundary conditions and higher accumulation simulated higher SMB (Figure S5; TraCE-21ka, MPI, and IPSL) and therefore resulted in a stronger magnitude and a wider swath of cold based ice conditions across the Adirondacks (Figure S4; TraCE-21ka, MPI, and IPSL). Such conditions are similar to what has been reported to exist across the thick ice divides of modern ice sheets (i.e., Greenland Ice Sheet; MacGregor et al., 2022), where in the absence of heat generation due to frictional heating, vertical advection of cold surface climate dictates the basal thermal state (Lai and Anders, 2021). We also find that frozen bed conditions existed across other areas of high bedrock relief during the LGM (Figure 3) where frozen bed patches are simulated above warm-based ice at lower elevations. Across both the White Mountains and Mount Katahdin (Figure 5&6), upstream ice flow slowed as it encountered resistance from the underlying high bedrock relief. Only where both ice velocity and thickness are relatively low, and bedrock elevation is high, is the presence of frozen bed conditions simulated. Where ice thickness and driving stresses increase downstream of these bedrock features, ice velocities increase and warm-based conditions are simulated. We note that while the impact of degree day factors is unexplored in this work, we expect this to have a limited influence on the simulated thermal characteristics of the LIS across the NE USA. During the LGM, monthly surface temperatures remain below freezing across the ice sheet interior, with exception of the Southern margin (Figure S5). Therefore, surface melt is limited across the ice sheet interior, and instead the prescribed surface temperature and accumulation are the primary

Formatted: Font: Not Italic

**Deleted:** Therefore, given that geologic and geomorphic indicators of LIS thermal conditions show that cold-based ice existed across areas of high relief in the NE USA (Goldthwait, 1940; Davis, 1989; Corbett et al., 2018; Halsted et al., 2023), we relied upon a downscaling procedure to ensure that the underlying bedrock relief and resulting stress balance was well resolved. Our results agree with geologic interpretations (Davis, 1989; Bierman et al., 2015; Halsted et al., 2023) that suggest the existence of polythermal ice across the NE USA during the LGM.

**Deleted:** is

**Deleted:** when looking at

**Deleted:** Our experiments relied on a small ensemble of simulated surface climate at the LGM from climate model experiments, each simulating a varying magnitude of LGM cooling and precipitation change.

**Deleted:** T

**Deleted:** using

**Deleted:** and which simulated

**Deleted:** ,

**Deleted:** simulated

**Deleted:** we observe

**Deleted:**

factors driving the simulated differences in the thermal conditions (Figure S5). Nevertheless, for simulations across the last deglaciation, the choice of degree day factors can have a large influence on the simulated ice history and ultimately the transient evolution of ice temperature as deglacial surface temperature and melt rise (Matero et al., 2020).

Regional geologic interpretations of isotopic data suggest that a thermal boundary between cold-based (low erosive) ice and warm-based (erosive ice) existed at ~1200 m across areas of high bedrock relief in the NE USA (Halsted et al., 2022). Yet, undated geomorphic indicators of warm-based ice on Mount Washington are found at 1680 m and 1820 m. Across Mount Katahdin and the White Mountains, we simulate a thermal boundary of 1320 m and 1530 m respectively, which is in reasonable agreement with the different geologic assessment.

Across the Adirondack Mountains, frozen bed conditions are simulated both in areas of high bedrock relief and lower elevation sites that reside under a simulated regional ice divide, making the interpretation more complicated. While the region wide thermal boundary is simulated to be at 880 m, if we only consider the High Peaks Area where geologic data of ice thinning exists (Barth et al., 2019), the thermal boundary resides at 1180 m. For high elevation sites, Barth et al. (2019) present an alternative hypothesis that the high-elevation TCN ages suggest early ice-sheet thinning ~20 ka in lieu of reflecting nuclide inheritance and that the regional thermal boundary likely existed above 1560 m. Nevertheless, our simulations confirm that this thermal boundary was not spatially constant, and instead varied geographically (Bierman et al., 2015; Corbett et al., 2018; Koester et al., 2021).

While our experiments offer a spatially high-resolution reconstruction of the LGM basal thermal conditions of the LIS across the NE USA, our methodology assumes that the LIS is in equilibrium with the LGM surface climate, which is likely not a true reflection of LGM conditions. It is noted that while Tarasov and Peltier (2007) simulate the LIS thermal state across the last glacial cycle and find that maximum areal coverage of frozen bed conditions occurred during the LGM, since the LIS experienced a transiently evolving climate prior to the LGM as the surface climate cooled, our simulations may reflect a colder thermal state than may have been experienced. Additionally, the spatially varying basal friction coefficient is constant and not thermodynamically coupled in our simulations. While this coupling has recently been shown to have greatest influence in areas of ice streaming across the LIS with attendant feedbacks on ice surface lowering and ultimately ice thickness, a thermodynamically coupled friction may promote colder basal conditions through feedbacks between ice flow, ice temperature, and basal friction (Moreno et al., 2023). Although we cannot fully address how these limitations and assumptions affect our results, since our simulations agree well with geologic interpretations that polythermal conditions and ultimately a regime of differential erosion existed across the NE USA, we attain a level of confidence that we are indeed simulating thermal conditions that generally reflected LGM conditions. However, future work should evaluate how these thermal conditions may have changed in response to deglacial LIS change as our contemporary assessment of geomorphic and geologic indicators likely integrates the full glacial and deglacial history.

Because the data derived from dipstick studies aimed at constraining vertical thinning histories can be difficult to interpret, our regional and local scale modeling framework may prove helpful for making more informed choices on sample site selection in places where model simulations suggest warm-based, and ultimately erosive ice conditions, such is currently being done for fieldwork in the Adirondack Mountains (Barker et al., 2024). Additionally, since the results presented here support broader geologic interpretations that polythermal ice conditions likely existed across the NE USA (Halsted et al., 2023), such output may be useful in

Deleted:

Formatted: Font: Not Italic

Formatted: Font: Not Italic

Commented [MOU2]: Aaron – Bierman suggests it is intro material – what should we do? This reads to me like a discussion point?

Deleted: Regional geologic interpretations support that a thermal boundary between cold-based (low erosive) ice and warm-based (erosive ice) existed at ~1200 m across areas of high bedrock relief in the NE USA (Halsted et al., 2022). Terrestrial cosmogenic nuclide (TCN) surface exposure ages from various peaks across the NE USA exhibit signs of nuclide inheritance which is interpreted to reflect inefficient erosion by previous ice coverage. TCN ages from the peaks of Mount Katahdin (ME), Mount Washington (NH), and Little Haystack Mountain (NH), exhibit signs of nuclide inheritance suggestive of a thermal boundary below those locations (Bierman et al., 2015). While warm-based ice indicators (e.g., roche moutonnée and lodgement till) are found on Mt. Washington between 1680 m and 1820 m, a lack of age control on those features means the timing of erosion relative to the LGM is inconclusive

Deleted: 18

Deleted: 2

Deleted: that agrees well with independent assessments from geologic reconstructions

Deleted: of the difficulties in conducting

geomorphological interpretations of differential erosion and relief generation as well as transport processes of glacial erratics from lower elevation, warm-based areas (Bierman et al., 2015). Lastly, such a frame work shows promise in applications to other regions of the LIS where geologic and geomorphic indicators suggest the existence of sharp thermal contacts and erosional history, such as across portions of Arctic Canada and Baffin Island (Marsella et al., 2000; Briner et al., 2006; 2014).

## 5. Conclusions

In this study, we use a numerical ice sheet model to simulate at high spatial resolution, steady-state LGM basal thermal conditions for the LIS across the NE USA and at 3 specific locations characterized by high bedrock relief. LGM climate boundary conditions are used from a small ensemble of climate model simulations, each with a varying degree of LGM cooling and precipitation change relative to preindustrial climate. Our results illustrate that during the LGM, the LIS across the NE USA was mainly warm-based and ultimately erosive, yet exhibited polythermal ice conditions, as simulations reveal that cold-based ice existed across this region in areas of high bedrock elevation and slow ice flow (i.e., ice divides). At local scales, we find that within the Adirondack Mountains, a regional ice divide is simulated during the LGM, characterized by low ice velocities (<15 m/yr) and a wide swath of cold-based ice that spans a large elevational range. Across the White Mountains and Mount Katahdin, ice velocities are generally higher, with cold-based ice conditions being simulated only amongst the highest elevation peaks. Where existing models (Marshall and Clark, 2002; Tarasov and Peltier, 2007; Gregoire et al., 2012) lack sufficient resolution to capture these features, we simulate a complex thermal regime that may have existed across this region reflective of the highly variable topography of the region.

The results presented here support the conclusions from a large dataset of TCN surface exposure ages that relate nuclide inheritance across high relief areas of the NE USA to the presence of cold-based and low erosive conditions sometime during the LGM and last deglaciation (Bierman et al., 2015; Koester et al., 2017; Barth et al., 2019; Corbett et al., 2018; Corbett et al., 2019; Koester et al., 2020; Halsted et al., 2022; Halsted et al., 2023). These studies largely support that a thermal boundary of ~1200 m in elevation separated cold-based ice at higher elevations and warm-based ice at lower elevations. While our simulations support this conclusion, they also illustrate that this thermal boundary was not spatially consistent and instead varied geographically. The existence of polythermal ice conditions across this region has implications with respect to glacial geomorphology, as the erosive character of the ice sheet is closely tied to the basal thermal regime. Since dipstick studies (Bierman et al., 2015; Koester et al., 2017; Barth et al., 2019; Corbett et al., 2019; Koester et al., 2020; Halsted et al., 2023) have the potential to provide critical constraints on paleo ice sheet thinning, yet interpretations can be hindered by the existence of cold-based ice (i.e. low erosion and thus nuclide inheritance), studies like this may aid in future study site selection (e.g. Briner et al., 2022; Barker et al., 2024) as this downscaling procedure can be applied to specific sites of interest. Additionally, this downscaling approach may be useful for geomorphological assessments in other areas of the LIS where polythermal conditions may have existed (Davis et al., 1999; Davis et al., 2006; Briner et al., 2014; Staiger et al., 2005), by providing another metric to evaluate landscape evolution.

## Code and data availability

Deleted: for the first time

Deleted: Additionally, the results here are supportive of lower latitude polythermal ice conditions existing across the LIS during the LGM (Bierman et al., 2015; Colgan et al., 2002).

The simulations performed for this paper made use of the open-source Ice-Sheet and Sea-level System Model (ISSM) and are publicly available at <https://issm.jpl.nasa.gov/> (Larour et al., 2012). Model output described in this study can be found at <https://doi.org/10.5281/zenodo.12665418> (Cuzzzone et al., 2024). This includes the simulated output of LGM ice velocity (x and y components as well), ice thickness, and the simulated thermal agreement for cold and warm-based ice across the NE USA, the Adirondack Mountains, the White Mountains, and Mount Katahdin.

**Author contributions.** JC, AB, and KB conceived the study. JC conducted the model setup and conducted the experiments with input from MM. JC analyzed model output with help from AB, KB, and MM. JC and AB wrote the manuscript with input from KB and MM.

**Competing interests:** The contact author has declared that none of the authors has any competing interests.

**Financial support:** This work was supported by a grant from the National Science Foundation, Division of Earth Science (EAR; grant no. 2133699).

## References

- Abe-Ouchi, A., Saito, F., Kageyama, M., Braconnot, P., Harrison, S. P., Lambeck, K., Otto-Bliesner, B. L., Peltier, W. R., Tarasov, L., Peterschmitt, J.-Y., Takahashi, K. 2015. Ice-sheet configuration in the CMIP5/PMIP3 Last Glacial Maximum experiments, *Geosci. Model Dev.*, 8, 3621–3637, <https://doi.org/10.5194/gmd-8-3621-2015>.
- Åkesson, H., Morlighem, M., Nisancioglu, K. H., Svendsen, J. J., Mangerud, J. 2018. Atmosphere-driven ice sheet mass loss paced by topography: Insights from modelling the south-western Scandinavian Ice Sheet, *Quaternary Sci. Rev.*, 195, 32–47, <https://doi.org/10.1016/j.quascirev.2018.07.004>.
- Antevs, J. T.. 1932. *Alpine zone of Mt. Washington Range, Merrill and Webber, Auburn, Maine, 118 p.*
- Aschwanden, A., Bueller, E., Khroulev, C., Blatter, H. 2012. An enthalpy formulation for glaciers and ice sheets, *J. Glaciol.*, 58, 441–457, <https://doi.org/10.3189/2012JoG11J088>.
- Balco, G., Schaefer, J. M. 2006. Cosmogenic-nuclide and varve chronologies for the deglaciation of southern New England, *Quaternary Geochronology*, 1, 15–28, <https://doi.org/10.1016/j.quageo.2006.06.014>
- Balter-Kennedy, A., Schaefer, J. M., Balco, G., Kelly, M. A., Kaplan, M. R., Schwartz, R., Oakley, B., Young, N. E., Hanley, J., and Varuolo-Clarke, A. M. 2024. The Laurentide Ice Sheet in southern New England and New York during and at the end of the Last Glacial Maximum – A cosmogenic-nuclide chronology, *EGUsphere* [preprint], <https://doi.org/10.5194/egusphere-2024-241>.
- Barker, K., Barth, A., Cuzzzone, J., Caffee, M. 2024. Filling in the gaps for Laurentide deglacial thinning in the Adirondack Mountains, New York USA. *Geologic Society of America, Northeastern Section 59<sup>th</sup> Annual Meeting*, Manchester, NH.
- Barth, A.M., Marcott, S.A., Licciardi, J.M., Shakun, J.D. 2019. Deglacial Thinning of the Laurentide Ice Sheet in the Adirondack Mountains, New York, USA, Revealed by <sup>36</sup>CL Exposure Dating. *Paleoceanography and Paleoclimatology*. 34, 946–953, <https://doi.org/10.1029/2018PA003477>

710 Bierman, P.R., Davis, P.T., Corbett, L.B., Lifton, N.A., Finkel, R.C. Cold-based Laurentide ice  
 711 covered New England's highest summits during the Last Glacial Maximum. 2015.  
 712 *Geology*. 43, 12, 1059-1062. <https://doi.org/10.1130/G37225.1>  
 713 Blatter, H.: Velocity and stress-fields in grounded glaciers: A simple algorithm for including  
 714 deviatoric stress gradients. 1995. *J. Glaciol.*, 41, 333–  
 715 344, <https://doi.org/10.3189/S002214300001621X>.  
 716 Bondzio, J. H., Seroussi, H., Morlighem, M., Kleiner, T., Rückamp, M., Humbert, A., Larour, E.  
 717 Y. 2016. Modelling calving front dynamics using a level-set method: application to  
 718 Jakobshavn Isbræ, West Greenland, *The Cryosphere*, 10, 497–  
 719 510, <https://doi.org/10.5194/tc-10-497-2016>.  
 720 Briner, J.P., Miller, G.H., Davis, P.T., Finkel, R.C. 2006. Cosmogenic radionuclides from  
 721 differentially weathered fjord landscapes support differential erosion by overriding ice  
 722 sheets. *Geological Society of America Bulletin*, 118, 406-420.  
 723 <https://doi.org/10.1130/B25716.1>  
 724 Briner, J.P., Lifton, N.A., Miller, G.H., Refsnider, K., Anderson, R., Finkel, R. 2014. Using in  
 725 situ cosmogenic  $^{10}\text{Be}$ ,  $^{14}\text{C}$ , and  $^{26}\text{Al}$  to decipher the history of polythermal ice sheets on  
 726 Baffin Island, Arctic Canada. *Quaternary Geology*. 19, 4-13.  
 727 <http://dx.doi.org/10.1016/j.quageo.2012.11.005>  
 728 Briner JP, Cuzzzone JK, Badgley JA, Young NE, Steig EJ, Morlighem M, Schlegel NJ, Hakim  
 729 GJ, Schaefer JM, Johnson JV, Lesnek AJ, Thomas EK, Allan E, Bennike O, Cluett AA,  
 730 Csatho B, de Vernal A, Downs J, Larour E, Nowicki S. 2020. Rate of mass loss from the  
 731 Greenland Ice Sheet will exceed Holocene values this century. *Nature*. 586(7827):70-74.  
 732 <https://doi.org/10.1038/s41586-020-2742-6>.  
 733 Briner, J. P., Walcott, C. K., Schaefer, J. M., Young, N. E., MacGregor, J. A., Poinar, K., Keisling,  
 734 B. A., Anandakrishnan, S., Albert, M. R., Kuhl, T., Boeckmann, G. 2022. Drill-site  
 735 selection for cosmogenic-nuclide exposure dating of the bed of the Greenland Ice Sheet,  
 736 *The Cryosphere*, 16, 3933–3948, <https://doi.org/10.5194/tc-16-3933-2022>.  
 737 Bromley, G. R., Hall, B. L., Thompson, W. B., Kaplan, M. R., Garcia, J. L., Schaefer, J.  
 738 M. 2015. Later glacial fluctuations of the Laurentide Ice Sheet in the White Mountains of  
 739 Maine and New Hampshire, U.S.A. *Quaternary Research*, 83(3), 522–  
 740 530. <https://doi.org/10.1016/j.yqres.2015.02.004>  
 741 Budd, W. F., Keage, P. L., and Blundy, N. A.: Empirical studies of ice sliding. 1979. *J. Glaciol.*,  
 742 23, 157–170, <https://doi.org/10.3189/S0022143000029804>.  
 743 Budd, W. F. and Smith, I. 1981. The growth and retreat of ice sheets in response to orbital  
 744 radiation changes, Sea Level, Ice, and Climatic Change, IAHS Publication No. 131. 369–  
 745 409.  
 746 Caron, L., Ivins, E. R., Larour, E., Adhikari, S., Nilsson, J., and Blewitt, G.: GIA model statistics  
 747 for GRACE hydrology, cryosphere and ocean science. 2018. *Geophys. Res. Lett.*, 45,  
 748 2203–2212, <https://doi.org/10.1002/2017GL076644>.  
 749 Choi, Y., Morlighem, M., Rignot, E., Wood, M. 2021. Ice dynamics will remain a primary driver  
 750 of Greenland ice sheet mass loss over the next century, *Commun. Earth Environ.*, 2,  
 751 26, <https://doi.org/10.1038/s43247-021-00092-z>.  
 752 Clark, P. U., Dyke, A. S., Shakun, J. D., Carlson, A. E., Clark, J., Wohlfarth, B., Mitrovica, J. X.,  
 753 Hostetler, S. W., McCabe, A. M., 2009. The Last Glacial Maximum. *Science*, 325, 710–  
 754 714, <https://doi.org/10.1126/science.1172873>.

Clark, P. U., Mix., A. C., 2002. Ice sheets and sea level of the Last Glacial Maximum. Quaternary Science Reviews, 21, 1-7.

Colgan, P.M., Bierman, P.R., Mickelson, D.M., Caffee, M.W., 2002, Variation in glacial erosion near the southern margin of the Laurentide Ice Sheet, south-central Wisconsin, USA: Implications for cosmogenic dating of glacial terrains: Geological Society of America Bulletin, v. 114, p. 1581–1591, <https://doi.org/10.1130/0016-7606>

Corbett, L. B., Bierman, P. R., Davis, P.T. 2016. Glacial history and landscape evolution of southern Cumberland Peninsula, Baffin Island, Canada, constrained by cosmogenic <sup>10</sup>Be and <sup>26</sup>Al. Geological Society of America Bulletin. v. 128(7-8), p. 1173-1192. doi.org/10.1130/B31402.1

Corbett, L. B., Bierman, P. R., Larsen, P., Stone, B. D., Caffee, M. W. 2017. Cosmogenic nuclide age estimate for Laurentide Ice Sheet recession from the terminal moraine, New Jersey, USA, and constraints on Latest Pleistocene ice sheet history. Quaternary Research. v. 87(3), p. 482-498. doi.org/10.1017/qua.2017.11

Corbett, L. B., Bierman, P. R., Wright, S., Shakun, J., Davis, P.T., Goehring, B., Halsted, C., Koester, A., Caffee, M., Zimmerman, S. 2018. Analysis of multiple cosmogenic nuclides constrains Laurentide Ice Sheet history and process on Mt. Mansfield, Vermont's highest peak, Quaternary Science Reviews. doi.org/10.1016/j.quascirev.2018.12.014

Corbett, L. B., Bierman, P. R., Wright, S. F., Shakun, J. D., Davis, P. T., Goehring, B. M., Halsted, C. T., Koester, A. J., Caffee, M. W., Zimmerman, S. R. 2019. Analysis of multiple cosmogenic nuclides constrain Laurentide Ice Sheet history and process on Mt. Mansfield, Vermont's highest peak. Quaternary Science Reviews, 205, 234–246. <https://doi.org/10.1016/j.quascirev.2018.12.014>

Cuffey, K. M. and Paterson, W. S. B. 2010. The physics of glaciers, 4th edn., Butterworth-Heinemann, Oxford, ISBN 9780123694614.

Cuzzone, J., Barth, A., Barker, K., Morlighem, M., Ice sheet model simulations reveal polythermal ice conditions existed across the NE USA during the Last Glacial Maximum, Zenodo [dataset], <https://doi.org/10.5281/zenodo.12665418>, 2024.

Cuzzone, J. K., Morlighem, M., Larour, E., Schlegel, N., and Seroussi, H. 2018. Implementation of higher-order vertical finite elements in ISSM v4.13 for improved ice sheet flow modeling over paleoclimate timescales, Geosci. Model Dev., 11, 1683–1694, <https://doi.org/10.5194/gmd-11-1683-2018>.

Cuzzone, J. K., Young, N. E., Morlighem, M., Briner, J. P., and Schlegel, N.-J. 2022. Simulating the Holocene deglaciation across a marine-terminating portion of southwestern Greenland in response to marine and atmospheric forcings, The Cryosphere, 16, 2355–2372, <https://doi.org/10.5194/tc-16-2355-2022>.

Cuzzone, J., Romero, M., and Marcott, S. A. 2024. Modeling the timing of Patagonian Ice Sheet retreat in the Chilean Lake District from 22–10 ka, The Cryosphere, 18, 1381–1398, <https://doi.org/10.5194/tc-18-1381-2024>.

Dalton, A. S., Margold, M., Stokes, C. R., Tarasov, L., Dyke, A. S., Adams, R. S., Allard, S., Arends, H. E., Atkinson, N., Attig, J. W., Barnett, P. J., Barnett, R. L., Batterson, M., Bernatchez, P., Borns, H. W., Breckenridge, A., Briner, J. P., Brouard, E., Campbell, J. E., Carlson, A. E., Clague, J. J., Curry, B. B., Daigneault, R.-A., Dub.-Loubert, H., Easterbrook, D. J., Franzi, D. A., Friedrich, H. G., Funder, S., Gauthier, M. S., Gowan, A. S., Harris, K. L., H. tu, B., Hooyer, T. S., Jennings, C. E., Johnson, M. D., Kehew, A. E., Kelley, S. E., Kerr, D., King, E. L., Kjeldsen, K. K., Knaeble, A. R., Lajeunesse, P.,

Formatted: Font: (Default) Times New Roman

Formatted: Font: (Default) Times New Roman

Formatted: Font: (Default) Times New Roman

Formatted: Font: (Default) Times New Roman



801 Lakeman, T. R., Lamothe, M., Larson, P., Lavoie, M., Loope, H. M., Lowell, T. V.,  
 802 Lusardi, B. A., Manz, L., McMartin, I., Nixon, F. C., Occhietti, S., Parkhill, M. A., Piper,  
 803 D. J. W., Pronk, A. G., Richard, P. J. H., Ridge, J. C., Ross, M., Roy, M., Seaman, A.,  
 804 Shaw, J., Stea, R. R., Teller, J. T., Thompson, W. B., Thorleifson, L. H., Utting, D. J.,  
 805 Veillette, J. J., Ward, B. C., Weddle, T. K., and Wright, H. E. 2020. An updated  
 806 radiocarbon-based ice margin chronology for the last deglaciation of the North American  
 807 Ice Sheet Complex, *Quaternary Sci Rev*, 234, 106223,  
 808 <https://doi.org/10.1016/j.quascirev.2020.106223>.  
 809 [Davis, P.T. 1978. Quaternary glacial history of Mt. Katahdin, Maine: implications for vertical](#)  
 810 [extent of the late Wisconsinian Laurentide ice, Geological Society of America and](#)  
 811 [Geological Association of Canada Joint Annual Meeting, Abstract with Program, v. 10,](#)  
 812 [n. 7, p. 386.](#)  
 813 Davis, P.T., 1989, Quaternary glacial history of Mt. Katahdin and the nunatak hypothesis, in  
 814 Tucker, R.D., and Marvinney, R.G., eds., *Studies in Maine geology*, Volume 6,  
 815 Quaternary geology: Augusta, Maine Geological Survey, p. 119–134.  
 816 Davis, P. T., Bierman, P. R., Marsella, K. A., Caffee, M. W., Southon, J. R. (1999). Cosmogenic  
 817 analysis of glacial terrains in the eastern Canadian Arctic: A test for inherited nuclides  
 818 and the effectiveness of glacial erosion. *Annals of Glaciology*, (28) 181-188.  
 819 <https://doi.org/10.3189/172756499781821805>.  
 820 Davis, P. T., Briner, J. P., Coulthard, R. D., Finkel, R. C., Miller, G. H. 2006. Preservation of  
 821 Arctic landscapes overridden by cold-based ice sheets. *Quaternary Research*, (65) 156-  
 822 163. <https://doi.org/10.1016/j.yqres.2005.08.019>  
 823 [De Laski, J. 1872. Glacial action on Mount Katahdin, American Journal of Science, v. 3, p. 27-](#)  
 824 [31.](#)  
 825 Dias dos Santos, T., Morlighem, M., and Brinkerhoff, D. 2022. A new vertically integrated  
 826 MOno-Layer Higher-Order (MOLHO) ice flow model, *The Cryosphere*, 16, 179–  
 827 195, <https://doi.org/10.5194/tc-16-179-2022>.  
 828 [Drebbler, J., Halsted, C., Corbett, L., Bierman, P., Caffee, M. 2023. In-situ cosmogenic 10Be](#)  
 829 [dating of Laurentide Ice Sheet retreat from central New England, USA, Geosciences](#)  
 830 [2023, 13\(7\), 213 doi.org/10.3390/geosciences13070213](#)  
 831 Dyke, A. S., 2004. An outline of North American Deglaciation with emphasis on central and  
 832 northern Canada. *Developments in Quaternary Sciences*, 2, 373-424,  
 833 [https://doi.org/10.1016/S1571-0866\(04\)80209-4](https://doi.org/10.1016/S1571-0866(04)80209-4).  
 834 Farr, T.G., E. Caro, R. Crippen, R. Duren, S. Hensley, M. Kobrick, M. Paller, E. Rodriguez, P.,  
 835 Rosen, L. Roth, D. Seal, S. Shaffer, J. Shimada, J. Umland, M. Werner. 2007. The Shuttle  
 836 Radar Topography Mission. *Reviews of Geophysics*, v. 45, RG2004,  
 837 <https://doi.org/10.1029/2005RG000183>.  
 838 Franzi D.A., Barclay, D.J., Kranitz, R., and Gilson, K., 2015, Quaternary deglaciation of the  
 839 Champlain Valley with specific examples from the Ausable River valley, in Franzi, D.A.,  
 840 (ed.), *Geology of the Northeastern Adirondack Mountains and Champlain–St. Lawrence*  
 841 *Lowlands of New York, Vermont and Quebec: Field Trip Guidebook, New York State*  
 842 *Geological*.  
 843 GEBCO Bathymetric Compilation Group 2021. 2021. The GEBCO\_2021 Grid – a continuous  
 844 terrain model of the global oceans and land, NERC EDS British Oceanographic Data  
 845 Centre NOC, <https://doi.org/10.5285/c6612cbe-50b3-0cff-e053-6c86abc09f8f>.

Formatted: Default Paragraph Font, Font: (Default) +Body (Calibri), Font color: Text 1, Pattern: Clear

Formatted: Font: (Default) Times New Roman

Formatted: Font: (Default) Times New Roman

- Goldthwait, R.P., 1940, *Geology of the Presidential Range, New Hampshire*: Concord, New Hampshire Academy of Sciences, 43 p.
- Goldthwait, R.P., 1970, *Mountain glaciers of the Presedential Range in New Hampshire, Arctic and Alpine Research*, v. 2, p. 85-102.
- Golledge, N. R., Thomas, Z. A., Levy, R. H., Gasson, E. G. W., Naish, T. R., McKay, R. M., Kowalewski, D. E., and Fogwill, C. J. 2017. Antarctic climate and ice-sheet configuration during the early Pliocene interglacial at 4.23 Ma, *Clim. Past*, 13, 959–975, <https://doi.org/10.5194/cp-13-959-2017>.
- Gregoire LJ, Payne AJ, Valdes PJ. 2012. Deglacial rapid sea level rises caused by ice-sheet saddle collapses. *Nature* 487:219–222. <https://doi.org/10.1038/nature11257>.
- Hall, B. L., Borns, H. W., Bromley, G. R. M., Lowell, T. V., 2017. Age of the Pineo Ridge System: Implications for behavior of the Laurentide Ice Sheet in eastern Maine, U.S.A., during the last deglaciation. *Quaternary Science Reviews*, 169, 344-356, <https://doi.org/10.1016/j.quascirev.2017.06.011>.
- Halsted, C., Bierman, P., Shakun, J., Davis, P. T., Corbett, L., Caffee, M., Hodgdon, T., Licciardi, J. 2022. Rapid southeastern Laurentide Ice Sheet thinning during the last deglaciation revealed by elevation profiles of in-situ cosmogenic  $^{10}\text{Be}$ , *GSA Bulletin*, [doi.org/10.1130/B36463.1](https://doi.org/10.1130/B36463.1)
- Halsted, C.T., Bierman, P.R., Shakun, J.D., Davis, T., Corbett, L.B., Caffee, M.W., Hodgdon, T.S., Licciardi, J.M. 2023. Rapid southeastern Laurentide Ice Sheet thinning during the last deglaciation revealed by elevation profiles of in situ cosmogenic  $^{10}\text{Be}$ . *GSA Bulletin*, 135, 7-8, 2075-2087. <https://doi.org/10.1130/B36463.1>
- He, F., Shakun, J. D., Clark, P. U., Carlson, A. E., Liu, Z., Otto-Bliesner, B. L., and Kutzbach, J. E. 2013. Northern Hemisphere forcing of Southern Hemisphere climate during the last deglaciation, *Nature*, 494, 81–85, <https://doi.org/10.1038/nature11822>
- Hersbach, H., Bell, B., Berrisford, P., Hirahara, S., Horányi, A., Muñoz-Sabater, J., Nicolas, J., Peubey, C., Radu, R., Schepers, D., Simmons, A., Soci, C., Abdalla, S., Abellan, X., Balsamo, G., Bechtold, P., Biavati, G., Bidlot, J., Bonavita, M., De Chiara, G., Dahlgren, P., Dee, D., Diamantakis, M., Dragani, R., Flemming, J., Forbes, R., Fuentes, M., Geer, A., Haimberger, L., Healy, S., Hogan, R. J., Hólm, E., Janisková, M., Keeley, S., Laloyaux, P., Lopez, P., Lupu, C., Radnoti, G., de Rosnay, P., Rozum, I., Vamborg, F., Villaume, S., and Thépaut, J.-N. 2020. The ERA5 global reanalysis, *Q. J. Roy. Meteor. Soc.*, 146, 1999–2049, <https://doi.org/10.1002/qj.3803>.
- Hooke, R.L., Fastook, J. Thermal conditions at the bed of the Laurentide ice sheet in Maine during deglaciation: implications for esker formation. *Journal of Glaciology*. 53. 183. 2007. <https://doi.org/10.3189/002214307784409243>
- Kageyama, M., Harrison, S. P., Kapsch, M.-L., Lofverstrom, M., Lora, J. M., Mikolajewicz, U., Sherrieff-Tadano, S., Vadsaria, T., Abe-Ouchi, A., Bouttes, N., Chandan, D., Gregoire, L. J., Ivanovic, R. F., Izumi, K., LeGrande, A. N., Lhardy, F., Lohmann, G., Morozova, P. A., Ohgaito, R., Paul, A., Peltier, W. R., Poulsen, C. J., Quiquet, A., Roche, D. M., Shi, X., Tierney, J. E., Valdes, P. J., Volodin, E., and Zhu, J. 2021. The PMIP4 Last Glacial Maximum experiments: preliminary results and comparison with the PMIP3 simulations, *Clim. Past*, 17, 1065–1089, <https://doi.org/10.5194/cp-17-1065-2021>.
- Koester, A. J., Shakun, J. D., Bierman, P. R., Davis, P. T., Corbett, L. B., Braun, D., Zimmerman, S. R. 2017. Rapid thinning of the Laurentide Ice Sheet in coastal Maine, USA, during late

Formatted: Font: (Default) Times New Roman

891 Heinrich Stadial 1. *Quaternary Science Reviews*, 163, 180–  
 892 192. <https://doi.org/10.1016/j.quascirev.2017.03.005>  
 893 Klemen, J., Hattestrand, C. Frozen-bed Fennoscandian and Laurentide ice sheets during the Last  
 894 Glacial Maximum. 1999. *Nature*. 402, 63-66, <https://doi.org/10.1038/47005>.  
 895 Klemen, J., Glasser, M.F. The subglacial thermal organization (STO) of ice sheets. 2007.  
 896 *Quaternary Science Reviews*. 26,5-6,585-597.  
 897 <https://doi.org/10.1016/j.quascirev.2006.12.010>  
 898 Koester, A. J., Shakun, J. D., Bierman, P. R., Davis, P. T., Corbett, L. B., Braun, D., Zimmerman,  
 899 S. R., 2017. Rapid thinning of the Laurentide Ice Sheet in coastal Maine, USA, during late  
 900 Heinrich Stadial 1. *Quaternary Science Reviews*, 163, 180-192,  
 901 <https://doi.org/10.1016/j.quascirev.2017.03.005>.  
 902 Koester, A. J., Shakun, J. D., Bierman, P. R., Davis, P. T., Corbett, Goehring, B. M., Vickers, A.  
 903 C., Zimmerman, S. R., 2021. Laurentide ice sheet thinning and erosive regimes at Mount  
 904 Washington, New Hampshire, inferred from multiple cosmogenic nuclides. Untangling the  
 905 Quaternary Period – A Legacy of Stephen C. Porter. *GSA Special Papers*.  
 906 Larour, E., Seroussi, H., Morlighem, M., and Rignot, E. 2012. Continental scale, high order, high  
 907 spatial resolution, ice sheet modeling using the Ice Sheet System Model (ISSM), *J.*  
 908 *Geophys. Res.-Earth*, 117, F01022, <https://doi.org/10.1029/2011JF002140>.  
 909 Lai, J. and Anders, A. M.: Climatic controls on mountain glacier basal thermal regimes dictate  
 910 spatial patterns of glacial erosion. 2021. *Earth Surf. Dynam.*, 9, 845–859,  
 911 <https://doi.org/10.5194/esurf-9-845-2021>.  
 912 Le Morzadec, K., Tarasov, L., Morlighem, M., and Seroussi, H. 2015. A new sub-grid surface  
 913 mass balance and flux model for continental-scale ice sheet modelling: testing and last  
 914 glacial cycle, *Geosci. Model Dev.*, 8, 3199–3213, [https://doi.org/10.5194/gmd-8-3199-](https://doi.org/10.5194/gmd-8-3199-2015)  
 915 2015.  
 916 Liu, Z., Otto-Bliesner, B., He, F., Brady, E., Tomas, R., Clark, P., Carlson, A., Lynch-Stieglitz, J.,  
 917 Curry, W., Brook, E., Erickson, D., Jacob, R., Kutzbach, J., Cheng, J.. 2009. Transient  
 918 simulation of last deglaciation with a new mechanism for Bølling-Allerød warming,  
 919 *Science*, 325, 310–314. <https://doi.org/10.1126/science.1171041>  
 920 MacGregor, J. A., Fahnestock, M. A., Catania, G. A., Aschwanden, A., Clow, G. D., Colgan, W.  
 921 T., Gogineni, S. P., Morlighem, M., Nowicki, S. M., Paden, J. D., and Price, S. F. 2016. A  
 922 synthesis of the basal thermal state of the Greenland Ice Sheet, *J. Geophys. Res.-Earth*,  
 923 121, 1328–1350.  
 924 MacGregor, J. A., Chu, W., Colgan, W. T., Fahnestock, M. A., Felikson, D., Karlsson, N. B.,  
 925 Nowicki, S. M. J., and Studinger, M.: GBaTSv2: a revised synthesis of the likely basal  
 926 thermal state of the Greenland Ice Sheet. 2022. *The Cryosphere*, 16, 3033–3049,  
 927 <https://doi.org/10.5194/tc-16-3033-2022>.  
 928 Marquette, G.C., Gray, J.T., Gosse, J.C., Courchesne, F., Stockli, L., Macpherson, G., Finkel, R.  
 929 2004. Felsenmeer persistence under non-erosive ice in the Tornqat and Kaumajet  
 930 mountains, Quebec, and Labrador, as determined by soil weathering and cosmogenic  
 931 nuclide exposure dating. *Canadian Journal of Earth Sciences*. 41, 1, 19-38.  
 932 <https://doi.org/10.1139/e03-072>  
 933 Matero ISO, Gregoire LJ, Ivanovic RF, Tindall JC, Haywood AM. 2017. The 8.2 ka cooling  
 934 event caused by Laurentide ice saddle collapse. *Earth Planet Sci Lett* 473:205–214.  
 935 <https://doi.org/10.1016/j.epsl.2017.06.011>

Marsella, K. A., Bierman, P. R., Davis, P. T., Caffee, M. W. 2000. Cosmogenic  $^{10}\text{Be}$  and  $^{26}\text{Al}$  ages for the last glacial maximum, eastern Baffin Island, Arctic Canada. *Geological Society of America Bulletin*. v. 112(8), p. 1296-1312. doi.org/10.1130/0016-7606(2000)112<1296:CBAAAF>2.0.CO;2

Marshall, S. J., Clark, P.U. 2002. Basal temperature evolution of North American ice sheets and implications for the 100-kyr cycle, *Geophys. Res. Lett.*, 29(24), 2214, https://doi.org/10.1029/2002GL015192.

Marshall, S.J., Tarasov, L., Clarke, G.K.C., Peltier, W.R. 2000. Glaciological reconstruction of the Laurentide Ice Sheet: physical processes and modelling challenges. *Canadian Journal of Earth Sciences*. 37, 5, 769-793. https://doi.org/10.1139/e99-113

Moreno-Parada, D., Alvarez-Solas, J., Blasco, J., Montoya, M., and Robinson, A. 2023. Simulating the Laurentide Ice Sheet of the Last Glacial Maximum, *The Cryosphere*, 17, 2139–2156, https://doi.org/10.5194/tc-17-2139-2023.

Morlighem, M., Bondzio, J., Seroussi, H., Rignot, E., Larour, E., Humbert, A., Rebuffi, S., Modeling of Store Gletscher's calving dynamics, West Greenland, in response to ocean thermal forcing. 2016. *Geophys. Res. Lett.*, 43, doi:10.1002/20116GL067695.

Pattyn, F. 2003. A new three-dimensional higher-order thermomechanical ice sheet model: Basic sensitivity, ice stream development, and ice flow across subglacial lakes, *J. Geophys. Res.*, 108, 2382, https://doi.org/10.1029/2002JB002329.

Pollard, D. and DeConto, R. M.: Description of a hybrid ice sheet-shelf model, and application to Antarctica. 2012. *Geosci. Model Dev.*, 5, 1273–1295, https://doi.org/10.5194/gmd-5-1273-2012.

Ridge, J. C., Balco, G., Bayless, R. L., Beck, C. C., Carter, L. B., Dean, J. L., Voytek, E. B., Wei, J. H., 2012. The New North American Varve Chronology: A Precise Record of Southeastern Laurentide Ice Sheet Deglaciation and Climate, 18.2-12.5 kyr BP, and Correlations with Greenland Ice Core Records. *American Journal of Science*, 312, 685-722, https://doi.org/10.2475/07.2012.01.

Rückamp, M., Humbert, A., Kleiner, T., Morlighem, M., and Seroussi, H.: Extended enthalpy formulations in the Ice-sheet and Sea-level System Model (ISSM) version 4.17: discontinuous conductivity and anisotropic streamline upwind Petrov–Galerkin (SUPG) method. 2020. *Geosci. Model Dev.*, 13, 4491–4501, https://doi.org/10.5194/gmd-13-4491-2020.

Seroussi, H., Morlighem, M., Rignot, E., Khazendar, A., Larour, E., and Mouginot, J. 2013. Dependence of greenland ice sheet projections on its thermal regime, *J. Glaciol.*, 59, 218, https://doi.org/10.3189/2013JoG13J054.

Seguinot, J., Rogozhina, I., Stroeven, A. P., Margold, M., and Kleman, J. 2016. Numerical simulations of the Cordilleran ice sheet through the last glacial cycle, *The Cryosphere*, 10, 639–664, https://doi.org/10.5194/tc-10-639-2016.

Shapiro, N. M. and Ritzwoller, M. H. 2004. Inferring surface heat flux distribution guided by a global seismic model: particular application to Antarctica. *Earth Planet. Sci. Lett.*, 223, 213–224, https://doi.org/10.1016/j.epsl.2004.04.011.

Smith-Johnsen, S., Schlegel, N.-J., de Fleurian, B., and Nisancioglu, K. H. 2020. Sensitivity of the Northeast Greenland Ice Stream to geothermal heat, *J. Geophys. Res.-Earth*, 125, e2019JF005252, https://doi.org/10.1029/2019JF005252.

Formatted: Font: (Default) Times New Roman

Formatted: Font: (Default) Times New Roman

980 Staiger, J.K., Gosse, J.C., Johnson, J.V., Fastook, J., Gray, J.T., Tockli, D.F., Stockli, L., Finkel,  
981 R. 2005. Quaternary relief generation by polythermal glacier ice. *Earth Surface*  
982 *Processes and Landforms*, 30, 1145-1159. <https://doi.org/10.1002/esp.1267>.  
983 Sugden, D.E. 1977. Reconstruction of the Morphology, Dynamics, and Thermal Characteristics  
984 of the Laurentide Ice Sheet at its Maximum. *Arctic and Alpine Research*, 9,1, 21-47.  
985 <https://doi.org/10.2307/1550407>  
986 Tarasov, L. and Peltier, R. W. 1999. Impact of thermomechanical ice sheet coupling on a  
987 model of the 100 kyr ice age cycle, *J. Geophys. Res.-Atmos.*, 104, 9517–9545.  
988 <https://doi.org/10.1029/1998JD200120>  
989 Tarasov, L., Peltier, W.R. 2007. Coevolution of continental ice cover and permafrost extent over  
990 the last glacial-interglacial cycle in North America. *J. Geophys. Res.* 112, F02508,  
991 <https://doi.org/10.1029/2006JF000661>.  
992 [Tarr, R.S., 1900, Glaciation of Mt. Ktaadn, Maine, Geological Society of America Bulletin, v. 11,](#)  
993 [p. 433-448.](#)  
994 [Thompson, W. B., Fowler, B. K. & Dorion, C. C., 1999, Deglaciation of the northwestern White](#)  
995 [Mountains, New Hampshire. Géographie physique et Quaternaire, 53\(1\), 59–77.](#)  
996 <https://doi.org/10.7202/004882ar>  
997 Tigchelaar, M., Timmermann, A., Friedrich, T., Heinemann, M., and Pollard, D. 2019. Nonlinear  
998 response of the Antarctic Ice Sheet to late Quaternary Sea level and climate forcing,  
999 *The Cryosphere*, 13, 2615–2631, <https://doi.org/10.5194/tc-13-2615-2019>  
1000 Tierney, J. E., Zhu, J., King, J., Malevich, S. B., Hakim, G. J., Poulsen, C. J., 2020. Glacial  
1001 cooling and climate sensitivity revisited. *Nature*, 584, 569-573,  
1002 <https://doi.org/10.1038/s41586-020-2617-x>.  
1003 Ullman, D. J., Carlson, A. E., LeGrande, A. N., Anslow, F. S., Moore, A. K., Caffee, M.,  
1004 Syverson, K. M., Licciardi, J. M., 2014. Southern Laurentide ice-sheet retreat  
1005 synchronous with rising boreal summer insolation. *Geology*, 43, 23-26,  
1006 <https://doi.org/10.1130/g36179.1>.  
1007  
1008  
1009  
1010  
1011  
1012  
1013  
1014  
1015  
1016  
1017  
1018  
1019  
1020  
1021  
1022  
1023  
1024  
1025

Deleted: ¶

1027  
1028

